Ultrasonics Sonochemistry 73 (2021) 105492

Contents lists available at ScienceDirect

Ultrasonics Sonochemistry

journal homepage: www.elsevier.com/locate/ultson

Mechanistic study of the gas-phase chemistry during the spray deposition of Zn(O,S) films by mass spectrometry

Yanpeng Fu [a,b,e,*], Sophie Gledhill [b,c], Christian-Herbert Fischer [b,d]

[a] School of Materials and Energy, Guangdong University of technology, Guangzhou, Guangdong 510006, China
[b] Helmholtz Zentrum Berlin, Hahn-Meitner Platz 1, 14109 Berlin, Germany
[c] Fraunhofer Institute for Solar Energy Systems, Heidenhofstraße 2, Freiburg 79110, Germany
[d] Freie Universität Berlin, Institute of Chemistry and Biology, Fabeckstr. 34-36, D-14195 Berlin, Germany
[e] Guangdong Provincial Key Laboratory of Photonics Information Technology, Guangzhou, Guangdong 510006, China

ARTICLE INFO

Keywords:
Proton-promoted decomposition
Aerosol assisted CVD
Zn(O,S)
Mass spectrometry
Decomposition mechanism

ABSTRACT

The mass spectrometer, is a powerful tool to identify species and investigate reactions in the gas phase. In this work, the mechanism of aerosol assisted chemical vapor deposition (AACVD) of Zn(O,S) films prepared from H_2S and zinc acetylacetonate ($Zn(acac)_2$) precursor solutions is elucidated by mass spectrometry. The thermochemical behavior of $Zn(acac)_2$ is investigated by characterizing the influence of the solvent (H_2O or ethanol), the pH value of the precursor solution and the effect of the reactant H_2S, and by tracking gaseous intermediate products using mass spectrometry. Based on these results, a proton-promoted thermolysis mechanism for the AACVD Zn(O,S) film formation is then proposed, which is initiated by the hydrolysis with H_2O as the first stage, followed either by the rearrangement with an intramolecular proton or by the reaction with an extramolecular proton to produce ZnO or Zn(O,S). A real time mass tracking of the AACVD process reveals that only an adequate amount of H_2S promotes the chemical gas-phase decomposition and sulfurization process, while an excess of H_2S depletes the gaseous $Zn(acac)_2$ concentration and consequently reduces the film growth rate. The knowledge of the thermal decomposition process helps to optimize synthesis conditions and to adjust film properties to meet the requirement of the application in chalcopyrite or kesterite thin film solar cells.

1. Introduction

Zn(O,S), a promising chalcogenide material, has attracted increasing attention as an effective, cost-efficient and non-toxic buffer layer in thin film solar cells. Here it is a favorable alternative to substitute the toxic CdS in the applications of chalcopyrite and kesterite based thin film solar cells [1–5].

Various techniques have been employed to prepare Zn(O,S) thin films, including chemical bath deposition [1,6,7], sputtering [2], electrodeposition [8], atomic layer deposition [9,10], and aerosol assisted chemical vapor deposition (AACVD) [3]. The AACVD Zn(O,S) buffered $Cu(In,Ga)(S,Se)_2$ based thin film solar cells reported by our group have reached a remarkable efficiency of 15.4% [3], which was comparable to the references with CdS-buffer. It is noteworthy that the intrinsic part of the ZnO window layer can be omitted by the application of the AACVD Zn(O,S) buffer. Therefore, it can avoid the breaking of vacuum for the P2 scribing (second scribing step) in monolithically integrated devices between i-ZnO and n-ZnO that is necessary for the regular solar module structure [3].

The electronic band alignment and interfacial properties of Zn(O,S) with the absorber layer depend upon various factors like deposition methods, thickness of film, and ratios of elemental compositions (O/S ratios) parameters which can be controlled by AACVD. Taking into account the optimization of the Zn(O,S) quality and the complexity of the AACVD process, a comprehensive understanding of the Zn(O,S) formation mechanisms is required. In this work, we use a mass spectrometer to track and analyze the reaction process. It is especially designed to study intermediates and products in gas phase reactions before the solid film deposition [11]. It allows the measurement of mass spectra but also the tracking of particular ions. We investigated the Zn(O,S) growth mechanism by this technique using various set-ups, solvents, additives and a temperature gradient in the reaction chamber. Here, zinc acetylacetonate ($Zn(acac)_2$) is applied as the precursor to prepare Zn(O,S) films due to its easy availability and its high volatility. Turgambaeva et al. [12,13]

* Corresponding author.
E-mail address: fuyanpeng@gdut.edu.cn (Y. Fu).

https://doi.org/10.1016/j.ultsonch.2021.105492
Received 24 December 2020; Received in revised form 31 January 2021; Accepted 2 February 2021
Available online 10 February 2021

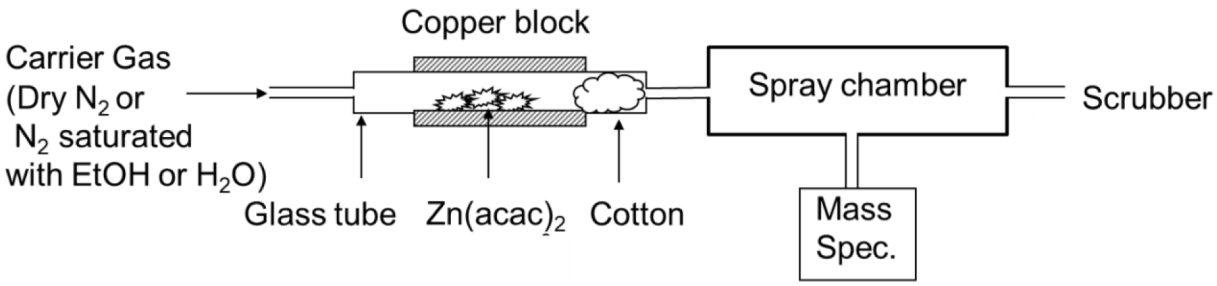

Fig. 1. Scheme of the experimental setup for the thermal analysis of $Zn(acac)_2$ powder by the mass spectrometer under various atmospheres, dry N_2, N_2 saturated with EtOH or N_2 saturated with H_2O.

used high temperature mass spectrometry to study the thermolysis and thermal stability of β-diketonates, such as $Sc(acac)_3$, $Pb(acac)_2$, $Al(acac)_3$, and $Cu(acac)_2$. Ismail et al. [14] investigated the thermolysis of $Zn(acac)_2$ by means of differential temperature analysis and thermogravimetry (TGA) and analyzed the products using IR-spectrometry and XRD. The influence of humidity on thermal decomposition of $Zn(acac)_2$ was also investigated by Arii et al. [15], using sample-controlled TGA, simultaneous differential scanning calorimetry and XRD, and TGA combined with evolved gas analysis by mass spectrometry.

Herein, mass spectrometry, which allows to analyze the gas phase in a simple and fast way, was introduced to study the formation mechanism of Zn(O,S) prepared from H_2S and $Zn(acac)_2$ solutions. First, the influence of solvent was elucidated by studying the thermal decomposition of $Zn(acac)_2$ powder under various atmospheres. Then, we studied the influence of H_2S and acid, followed by analyzing the gaseous intermediate products during the AACVD Zn(O,S) formation. A proton-promoted thermolysis mechanism was then proposed based on these studies. Finally, a real time mass tracking in the AACVD process was investigated.

2. Experimental section

2.1. Instrumentation

The spray chamber was mounted with a Hiden HPR60 quadrupole molecular beam mass spectrometer, which was a compact, mobile gas analysis system. The molecular beam sampling system, which was custom built and different from most of the mass spectrometers with high vacuum, worked at standard pressure and had 3 vacuum chamber system. It was available from Hiden Analytical. Scanning Electron

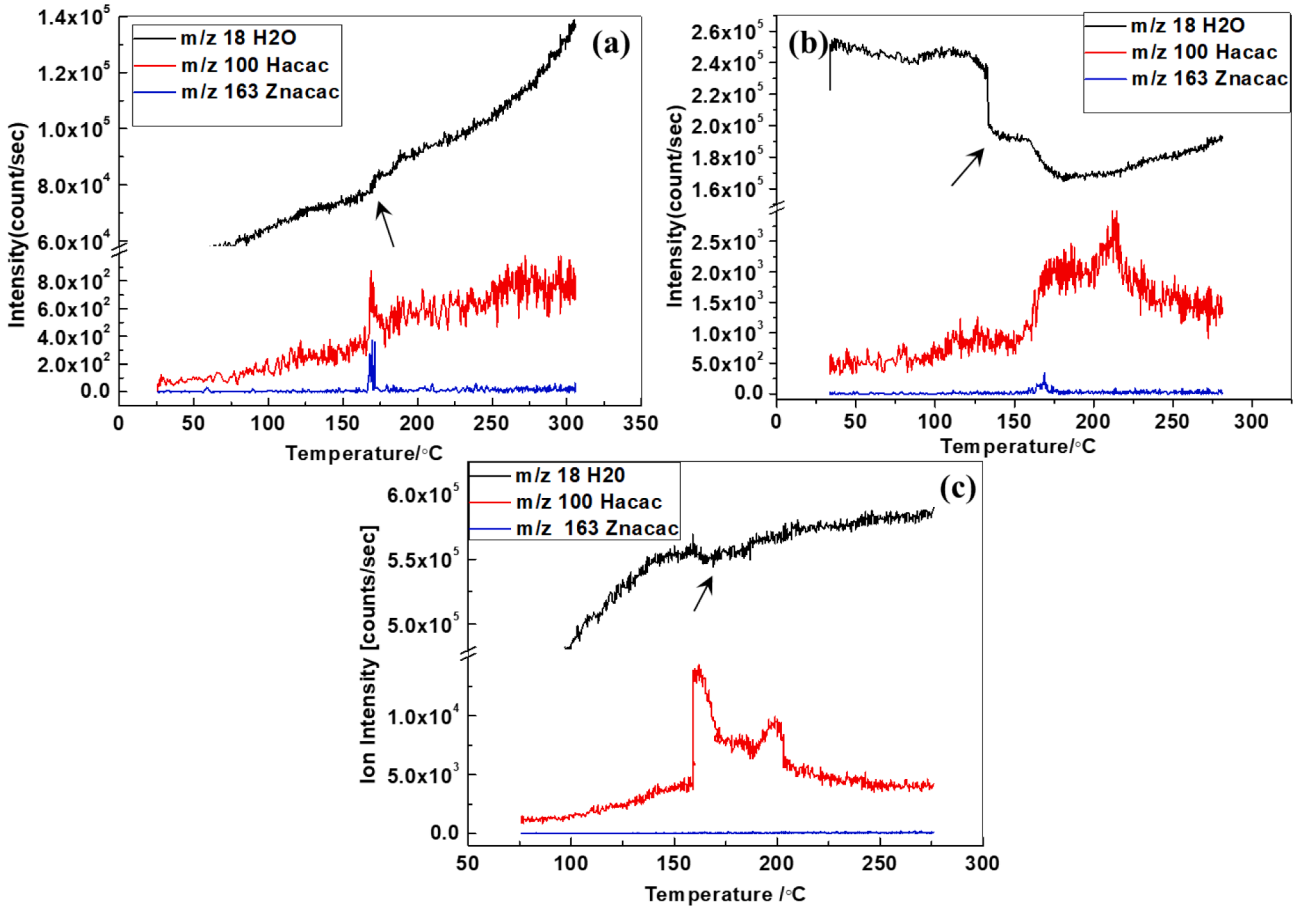

Fig. 2. Mass spectra tracking ions of H_2O^+ (*m/z* 18) in black, $Znacac^+$ (*m/z* 163) in red and $Hacac^+$ (*m/z* 100) in blue as a function of temperature upon heating the $Zn(acac)_2$ powder under different atmospheres. (a) dry N_2, (b) N_2 saturated with EtOH, and (c) N_2 saturated with H_2O·H_2O^+ depletion at about 170 °C is indicated with arrows. (For interpretation of the references to colour in this figure legend, the reader is referred to the web version of this article.)

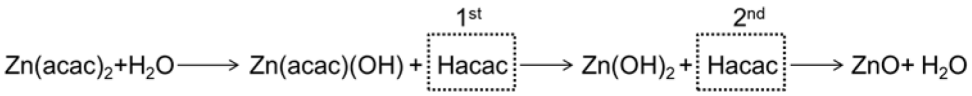

Micrographs (SEM) were measured applying FEG-SEM Leo1530 Gemini.

2.2. Thermal pyrolysis process of $Zn(acac)_2$ powder under various atmospheres

The scheme of the apparatus applied to study the thermal pyrolysis of $Zn(acac)_2$ (Alfa Aesar, ≥98%) was shown in Fig. 1. A glass tube containing $Zn(acac)_2$ powder was heated. N_2 stream carried the gaseous species to the attached mass spectrometer. A wad of glass wool adjacent to the $Zn(acac)_2$ powder, was used to prevent particles from reaching the measurement chamber. To guarantee the accurate temperature measurements, a thermocouple was placed at the bottom of the glass tube. Hence, the gaseous species produced as a function of temperature could be detected by the mass spectrometer. In other experiments, N_2 gas was bubbled through ethanol (abs. ≥99.8%) or H_2O in order to study the effect of these solvents.

2.3. Thermal pyrolysis process of $Zn(acac)_2$ solution

An aqueous or alcoholic $Zn(acac)_2$ solution was sprayed using a 1.6 MHz ultrasonic atomizer into micron-sized aerosol droplets, which were then fed by N_2 into the heated reaction chamber and mass spectrometer. H_2S was introduced simultaneously to study its effect on the thermolysis process. The concentration of $Zn(acac)_2$ solution was 25 mM, same as the one for the preparation of Zn(O,S) films. The reactor temperature was kept at 200 °C, identical to the one during the Zn(O,S) deposition. The gaseous species during spraying of $Zn(acac)_2$ solutions were recorded by the mass spectrometer. The aqueous solutions with different pH values of 3 and 6 were adjusted by acetic acid (Alfa Aesar, ≥99.7%).

2.4. Real time MS tracking of the AACVD process

The characteristic ions H_2S^+ (m/z 34), $Zn(acac)^+$ (m/z 163) and $Hacac^+$ (m/z 100) were recorded as a function of the H_2S concentration. The N_2 flow rate was kept at 2.5 ml/min. Various H_2S flow rates, 0, 5, 15, 30 and 45 ml/min, corresponding to the different H_2S/inert gas ratios of 0%, 0.01%, 0.03%, 0.06% and 0.09% were introduced simultaneously to study to the influence of the H_2S concentration.

3. Results and discussions

3.1. Thermal analysis of $Zn(acac)_2$ powder

To study the influence of the solvent during the Zn(O,S) thin film deposition, $Zn(acac)_2$ hydrate powders were heated-up from room temperature to 275 °C under various atmospheres while the gas phase was analyzed by mass spectrometry. According to the mass spectra shown by Macdonald [16], and the NIST-MS database [17,18], the Zn $(acac)_2$ mass spectrum includes two sets of fragmentations. One is from acetylacetone (Hacac) including m/z 100, 85, 72, 58, 43, 29, 15, and the other is from anhydrous $Zn(acac)_2$ including m/z 262, 247, 205, 163, 64. Therefore, the changes of the intensities of the characteristic ions $Hacac^+$ (m/z 100) and $Znacac^+$ (m/z 163) as a function of the temperature were tracked. Additionally, the ion H_2O^+ (m/z 18) was studied since the humidity was found to influence the decomposition process and its consumption indicates also a hydrolysis [15].

Fig. 2 displays the thermal-chemical behavior of $Zn(acac)_2$ powder at three different atmospheres, i.e. a) dry N_2, b) N_2 saturated with EtOH and c) N_2 saturated with H_2O. Below 120 °C, the crystal water of Zn $(acac)_2$ evaporates and explains the high level of the H_2O^+ signal even in the two experiments without water vapor in the carrier gas. It should be noted that the H_2O^+ signal intensity in the presence of EtOH vapor is about four times higher than with pure N_2. This can be explained in terms of a water/alcohol azeotrope formation accelerating the water evaporation. At around 120 °C, the hydrolysis of melted $Zn(acac)_2$ (melting point 124–126 °C) with crystal water leads to a slow increase of the $Hacac^+$ signal and a retarded increase or even a decrease in the H_2O^+ signal with temperature as observed especially with N_2 saturated with EtOH in Fig. 2b. With dry N_2, weak $Zn(acac)^+$ and $Hacac^+$ signals appear (Fig. 2a) at around 170 °C. The generation of gaseous $Zn(acac)_2$ and Hacac indicates that the evaporation and thermal decomposition processes coexist upon heating $Zn(acac)_2$ powder under dry N_2 atmosphere, which is in good agreement with the previous report [15]. As the temperature increases, the $Hacac^+$ signal gradually increases, revealing only a slow acceleration of the decomposition process upon heating whereas the $Zn(acac)^+$ signal vanishes. Obviously, at higher temperature the decomposition is faster than the evaporation and therefore the evaporated $Zn(acac)_2$ is immediately converted.

With the carrier gas of N_2 saturated with EtOH, both $Zn(acac)_2^+$ and $Hacac^+$ signals emerge as well at about 170 °C in Fig. 2b. At around 200 ± 10 °C, another $Hacac^+$ peak appears. The pair of the $Hacac^+$ peaks above 170 °C becomes stronger with the carrier gas of N_2 saturated with H_2O in Fig. 2c. The H_2O^+ depletion at 170 °C (indicated with arrows in Fig. 2a-c) occurs synchronously with the appearance of the positive $Hacac^+$ signal, indicating that H_2O vapor is consumed for the evolution of Hacac in the first reaction step. At 200 ± 10 °C it follows an additional Hacac formation without evidence of water consumption. Therefore, we propose that gaseous $Zn(acac)_2$ first hydrolyzes with H_2O resulting in the first evolution of Hacac at 170 °C. then it further decomposes to ZnO with the second evolution of Hacac at around 200 °C, which is described in the following equation:

This proposal explains the reason why the controlled humidity accelerates the decomposition of $Zn(acac)_2$ in the literatures [19–21].

It should be noted that the signal intensity of $Hacac^+$ with the carrier gas of N_2 saturated with EtOH at 170 °C is several times stronger than the one with dry N_2, while the intensities of $Zn(acac)^+$ in both cases are in the same range. However, in order to produce more Hacac it needs more gaseous $Zn(acac)_2$. Thus, the alcohol must have a carrier effect for $Zn(acac)_2$. This could be an intermediate formation of a more volatile complex as shown for $InCl_3$ [22] or of an azeotrope which promotes evaporation analogous to the water steam distillation. But if we see here the same $Zn(acac)_2$ concentration as in the pure N_2 case, it is no contradiction and indicates that the gaseous hydrolysis in the presence of EtOH at 170 °C is also much faster than without. This correlates well with the quite distinct H_2O^+ depletion in this experiment (Fig. 2b). The reason for the faster hydrolysis can be a catalysis by the very weak Brønsted acid EtOH. This effect together with the higher yield of Zn $(acac)_2$ vapor lead therefore to more Hacac and to more H_2O consumption. On the other hand, it is clear that the H_2O vapor concentration in this case is less than in N_2 saturated with H_2O. In the latter experiment, one cannot observe the $Zn(acac)^+$ signal in Fig. 2c. It is suggested that the saturated H_2O vapor in the N_2 speeds up the decomposition of $Zn(acac)_2$ and therefore the consumption of $Zn(acac)_2$, that no steady state concentration can be established.

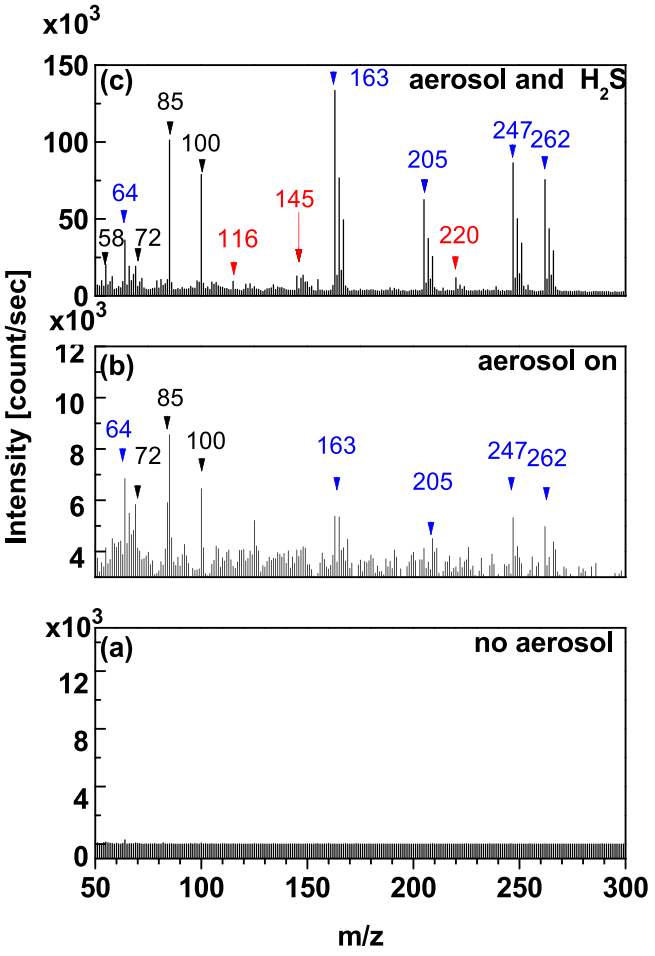

Fig. 3. Mass spectra of the background in the chamber (a), the alcoholic Zn $(acac)_2$ solution nebulized without (b) and with (c) H_2S. The chamber was kept at 200 °C. The black symbols correspond to the fragmentations of Hacac; the blue symbols list the set of $Zn(acac)_2$ fragments; the red symbols display the new emerging ions corresponding to the intermediate products in the presence of H_2S. (For interpretation of the references to colour in this figure legend, the reader is referred to the web version of this article.)

4. In-situ mass spectrum investigation during the AACVD Zn(O, S) deposition

4.1. Influence of H_2S

In order to investigate the reaction mechanism, the gaseous species during the AACVD Zn(O,S) deposition from H_2S and $Zn(acac)_2$ alcoholic solution at 200 °C were studied using in-situ mass spectroscopy.

Fig. 3a is the background mass spectrum before the aerosol generation. The spectra recorded during spraying the solution with and without H_2S are shown in Fig. 3b and c, respectively. According to the NIST database, the evolved gases during nebulizing the $Zn(acac)_2$ solution without H_2S are designated as a mixture of $Zn(acac)_2$ (*m/z* 64, 163, 205, 247, 262) and Hacac (*m/z* 72, 85, 100) [17,18]. The molecular ion $Zn(acac)_2)^+$ (*m/z* 262) undergoes the fragmentations to Zn^+ (*m/z* 64), $Zn(acac)^+$ (*m/z* 163) and others. The two sets of ions imply that the thermal decomposition is not fast enough to convert all $Zn(acac)_2$ under these conditions.

When H_2S is added to the system, the intensities of both sets of ions are around10-fold stronger in comparison to the H_2S-free system. Additionally, there are some new ions at *m/z* 220, 145 and 116, which could be attributed to the sulfur substitution of oxygen in the particular fragment. For example, the ions *m/z* 220 and 116 are proposed to be the intermediate products and could be assigned to $C_7H_8OSZn^+$ and $C_5H_8OS^+$, that are the sulfur substitutions of $C_7H_8O_2Zn^+$ ($Zn(acac)^+$) and $C_5H_8O_2^+$ ($Hacac^+$). Fig. S1 shows an example how H_2S attacks the $C_5H_8O_2^+$ ions. The difference between the presence and absence of H_2S clearly shows that H_2S does not only convert ZnO to Zn(O,S), but also participate in the $Zn(acac)_2$ thermolysis process. Table 1 lists the fragmentations in the mass spectrum and the corresponding assignments during nebulizing the $Zn(acac)_2$ alcoholic solution.

Table 1
The fragmentations in the mass spectra and the corresponding assignments during spraying the $Zn(acac)_2$ alcoholic solution in Fig. 3.

		m/z	Assignment
Presence and absence of H_2S	$Zn(acac)_2$	262	$C_{10}H_{14}O_4Zn^+$
		247	$C_9H_{11}O_4Zn^+$
		205	$C_7H_9O_3Zn^+$
		163	$C_5H_7O_2Zn^+$
		64	Zn^+
	Hacac	100	$C_5H_8O_2^+$
		85	$C_4H_5O_2^+$
		72	$C_4H_8O^+$
		58	$C_2H_6CO^+$
Presence of H_2S		220	$C_7H_8OSZn^+$
		145	fragment of *m/z* 163
		116	$C_5H_8OS^+$

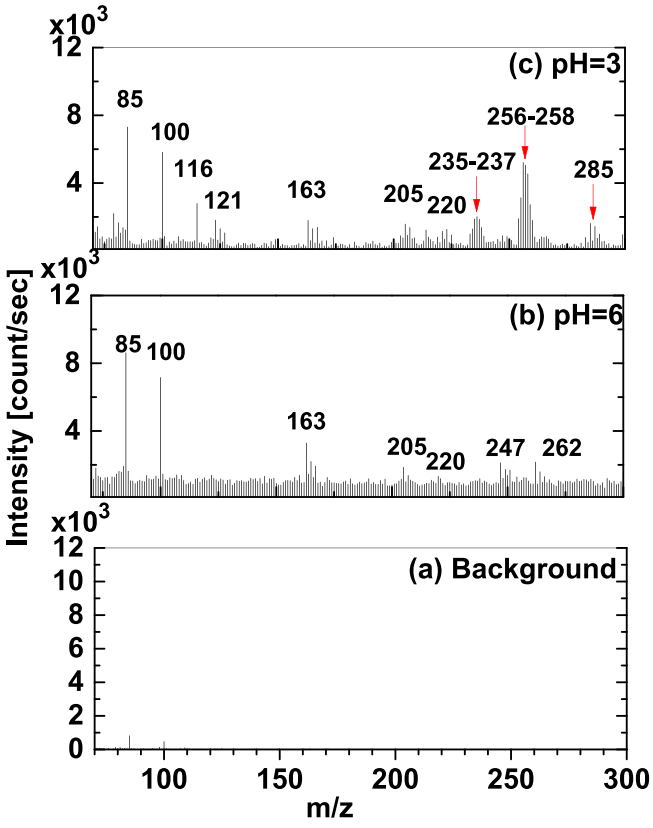

Fig. 4. Mass spectra of the gas phase during the nebulization of an aqueous Zn $(acac)_2$ solution with the simultaneous introduction of H_2S. (a) background, (b) pH = 6 aqueous solution, and (c) pH = 3 aqueous solution. The red arrows list the new emerging ions corresponding to the Zinc acetate fragments as compared to Fig. 3b. (For interpretation of the references to colour in this figure legend, the reader is referred to the web version of this article.)

4.1.1. Influence of acid

To investigate the effect of acid on the thermolysis process, we compared aqueous solutions of two different pH values adjusted by

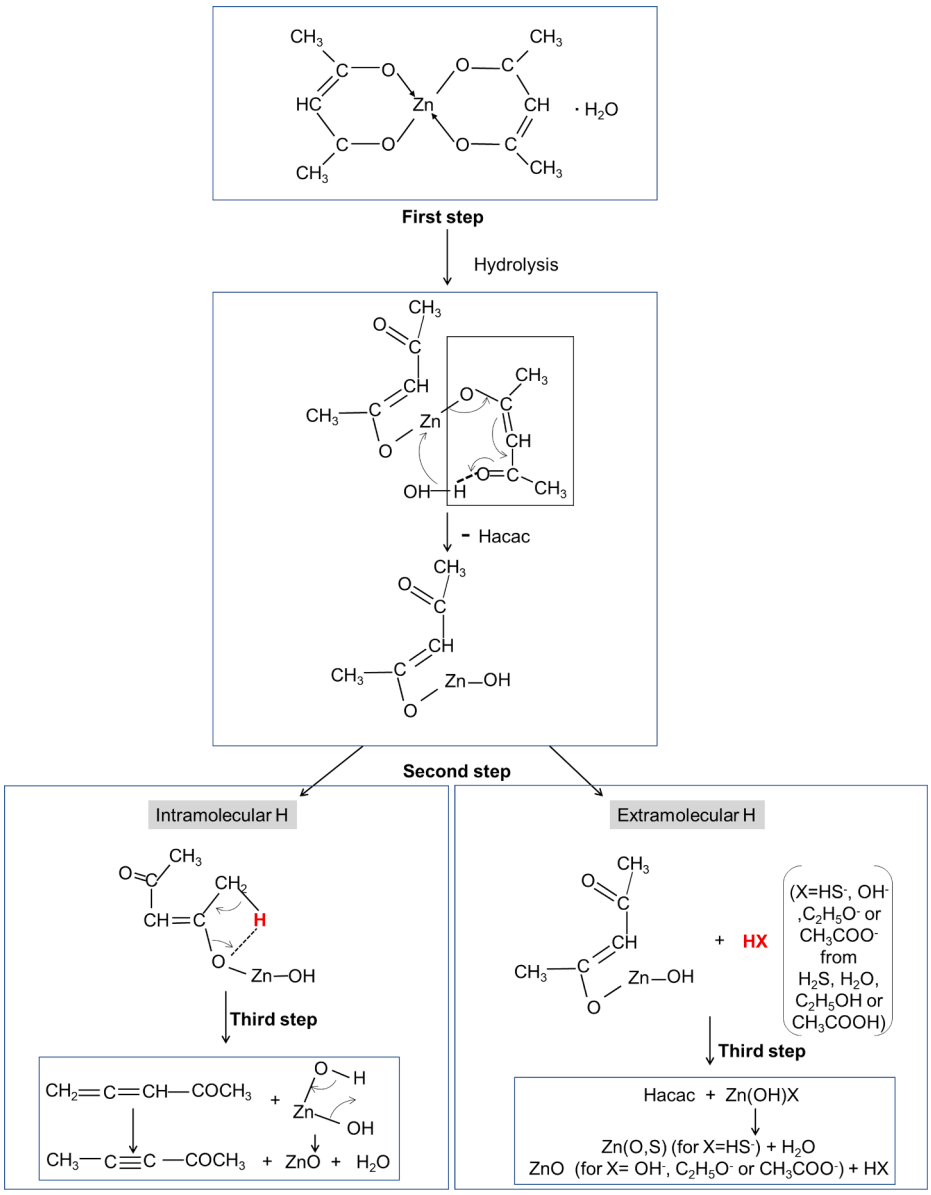

Fig. 5. Scheme of the $Zn(acac)_2$ thermal decomposition pathway on the hot substrate. The bond angles and lengths are not drawn to scale.

addition of acetic acid (HAc) to aqueous $Zn(acac)_2$ solutions. The gaseous species during the nebulization in the presence of H_2S are recorded by in-situ mass spectroscopy (Fig. 4). The background measurement is presented for comparison in Fig. 4a.

As can be seen in Fig. 4b, the detected ions during the nebulization of the $Zn(acac)_2$ solution of pH = 6 resemble the one of alcoholic $Zn(acac)_2$ solution in Fig. 3b except for the weaker peak intensities. This means, the accelerating effect of alcohol is missing, but the proton concentration is still too low to compensate it. A few ions, for instance *m/z* 145 and 116 cannot be detected. At pH = 3, we observe some new ions in Fig. 4c, e.g. *m/z* 285, 256–258 and 235–237, which could be ascribed to Zinc acetate ($Zn(ac)_2$) fragments [23]. The assignments of these new ions are listed in Table S1. It needs further study where the fragments stem from, either from the rearrangement of $Zn(acac)_2$ or from $Zn(ac)_2$, which is the product of the direct reaction between $Zn(acac)_2$ and HAc. The presence of zinc acetato complexes in the $Zn(acac)_2$ solution was reported at pH < 2 by Vacassy et al. [24] The intensities of the zinc containing ions, which are easily recognized by the isotopic multiplet, are much stronger at pH = 3 than the ones at pH = 6 despite the same concentration of the starting $Zn(acac)_2$ precursor solution. Therefore, the decomposition process is clearly accelerated by the presence of acids, which agrees well with the higher particle density in the deposited films at pH = 3 than the one at pH = 6 as seen in SEM images in Fig. S2.

4.1.2. *Proton-promoted thermolysis mechanism*

Based on the above study, we propose a 3-step thermal decomposition pathway of $Zn(acac)_2$ vapor on the hot substrate by taking into account the influences of H_2O, EtOH, H_2S and acid.

When the aerosol droplets pushed by the carrier gas approach the hot substrate surface, the following processes take place as the temperature increases: In the 1st step, the solvent and $Zn(acac)_2$ evaporate. The cyclic chelate bonds are opened (Fig. 5). Hydrolysis of $Zn(acac)_2$ takes place by reaction with water either from the solvent if this is water, if not with the crystal water forming Zn(acac)(OH) and Hacac. The proposal is supported by the Hacac peak at around 170 °C in the mass track when heating up $Zn(acac)_2$ powder and the more or less pronounced dip in the H_2O^+ track. (Fig. 2a-c).

The 2nd step can be an intra- or extra- molecular reaction. Without an extra proton in the system, the Zn(acac)(OH) disassembles by an intramolecular proton migration from one methyl group (marked in red

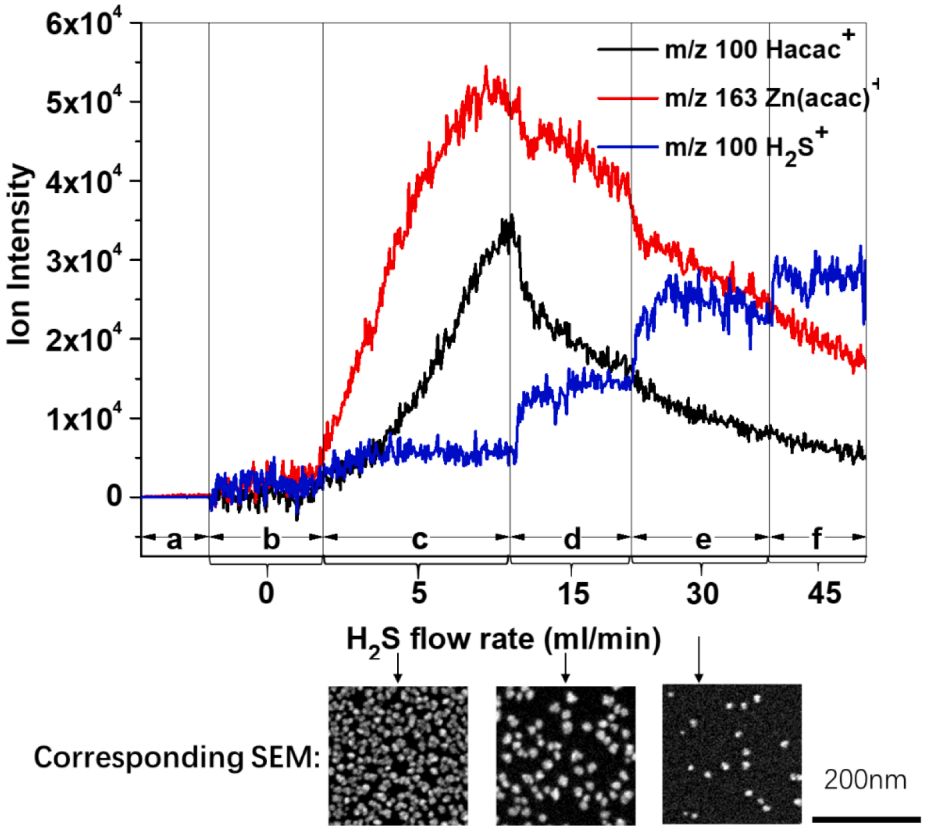

Fig. 6. Real time mass spectrum tracking of the ions of Znacac$^+$ (*m/z* 163), Hacac$^+$ (*m/z* 100) and H_2S^+ (*m/z* 34) as a function of the H_2S flow rate during the AACVD process. (a) background; nebulizing the precursor solution with different H_2S flow rates (b) 0; (c) 5 ml/min; (d) 15 ml/min; (e) 30 ml/min; and (f) 45 ml/min. The SEM images of the films acquired at the corresponding H_2S flow rates are represented below the mass tracks.

in Fig. 5) to oxygen of the Zn-O group with the formation of $Zn(OH)_2$ and a cumulene group, a tautomer of the correspondent acetylene. Though four-membered rings are not very favored transition states due to their strains, they are described in the literature. [25,26] $Zn(OH)_2$ will further pyrolyze with the formation of ZnO and H_2O in the last 3rd step, while the unstable cumulene decomposes to smaller molecules upon heating, such as acetone, carbon dioxide and so on. Without extra protons, there is only one step evolution of Hacac, which is consistent with only one pronounced Hacac peak in the mass track in Fig. 2a, where $Zn(acac)_2$ powder was heated with dry N_2.

Otherwise, if there are extramolecular protons in the system during the 2nd step, which could origin from H_2O, EtOH, H_2S, acid, etc., the Zn(acac)(OH) spiece favors to react with the extra protons to form the Zn-containing intermediate products and Hacac (Fig. 5) rather than to disassemble by the intramolecular proton migration. The Zn-containing intermediate products can further decompose to ZnO or Zn(O,S), repectively. The process is regarded as a proton-promoted thermolysis. Taking H_2O as an example, the $Zn(acac)^+(OH)^-$ group prefers to hydrolyze with the proton of H_2O with the formation of Hacac and $Zn(OH)_2$. Therefore, $Zn(acac)_2{\cdot}H_2O$ pyrolyzes with a second evolution of Hacac in the presence of the extramolecular proton. The proposed proton-promoted thermolysis mechanism is in good agreement with the experimental detection of two peaks at 170 and 200 °C in the Hacac mass track in Fig. 2b and c, where $Zn(acac)_2$ powder was heated with N_2 saturated with EtOH or H_2O. When compared to the intramolecular protons, the interaction with the extramolecular protons offers an extra pathway for the thermolysis of the $Zn(acac)^+(OH)^-$ group. It is more effective because the strain of the four-membered ring transition state is avoided. Therefore, the presence of protons, such as H_2O, EtOH, H_2S, acid, etc., promote the thermolysis of $Zn(acac)_2$ and evolution of Hacac.

The proposed proton-promoted thermolysis mechanism explains the observed phenomena upon heating $Zn(acac)_2$ powder in Fig. 2a-c, where H_2O^+ depletions appear simultaneously with an increasing Hacac$^+$ signal because the thermolysis of $Zn(acac)_2$ consumes H_2O in the system. In addition, this thermolysis mechanism gives a good interpretation of the experimental detection of two peaks at 170 and 200 °C in the Hacac mass track in Fig. 2b and c, where $Zn(acac)_2$ powder was heated with N_2 saturated with H_2O or EtOH, while there is only one peak upon heating with dry N_2 in Fig. 2a. Furthermore, it can be anticipated that in the presence of H_2S the higher intensities of zinc containing fragments and of Hacac represent the faster $Zn(acac)_2$ thermolysis in Fig. 3 due to the additional pathway involving external protons. This is in agreement with the faster experimental growth rate for Zn(O,S) than ZnO by AACVD. Last, the acceleration of the decomposition rate with the low pH value precursor solution can be well understood with the proton-promoted thermolysis mechanism.

4.2. *Real-time tracking of the AACVD process for the deposition of Zn(O, S)*

In this section, the mass spectrometer was used to track the AACVD process in real-time. The intensities of $Zn(acac)^+$ (*m/z* 163), Hacac$^+$ (*m/z* 100) and H_2S^+ (*m/z* 34) were tracked as a function of the H_2S flow rate. The carrier gas N_2 was kept at a constant flow rate of 2.5 ml/min, i.e. the H_2S concentration was easily varied. The precursor solution for the deposition of Zn(O,S) films could either be aqueous or alcoholic Zn (acac)2 solution. Here, the aqueous $Zn(acac)_2$ solution with pH = 3 was chosen as an example to study the effect of the H_2S.

At the beginning, only aerosol without H_2S is blown by N_2 into the chamber which is connected with the mass spectrometer. The latter detects only weak signals in Fig. 6. Only a few ZnO particles are obtained as seen in the SEM image without simultaneous introduction of H_2S in

Fig. S3. When a low H_2S concentration is established by introducing simultaneously 5% H_2S/Ar (5 ml/min) to the chamber, the intensities of both ions $Zn(acac)^+$ (*m/z* 163) and $Hacac^+$ (*m/z* 100) drastically increase. Nevertheless, these two intensities gradually decline with the further increasing H_2S/Ar flow rate, i.e. from 5 to 15, then to 30, and finally to 45 ml/min as indicated in Fig. 6. The SEM images of the Zn(O, S) films at different H_2S flow rates after 20 min by the AACVD process are exhibited below the mass tracks. The particle densities of the obtained films decrease with the increasing H_2S flow rate, which agrees well with the observed ion intensities of $Hacac^+$ (*m/z* 100) and $Zn(acac)^+$ (*m/z* 163) in Fig. 6 and therefore with the corresponding reactant concentration in the gas phase. The intensity descent is due to the dispersed Zn(O,S) particle formation due to the reaction between H_2S and $Zn(acac)_2$ already before arriving at the substrate surface. These particles do not stick at the substrate unlike particles which grow only on the substrate beginning with nuclei thus interlocking with the surface. This leads to a decrease in the deposition rate therefore resulting finally in a lower particle density of the AACVD Zn(S,O) films on the hot substrate. It does not concern the conversion rate, but the particles dispersed in the gas are lost.

5. Conclusion

In this work, we elucidate comprehensively the AACVD processes in the gas phase for the deposition of Zn(O,S) films prepared from H_2S and $Zn(acac)_2$ solution by means of mass spectrometry. The coexistence of the evaporation and decomposition processes observed by the mass spectrometry study confirms the AACVD mechanism. The process is referred to a proton-promoted thermolysis based on experiments and discussions on the influence of H_2O, EtOH, H_2S and pH value of the precursor solution as well as on the fragments detected by in-situ mass spectroscopy. The $Zn(acac)_2$ precursor molecules hydrolyze with one molecule H_2O and form Zn(acac)(OH) species and Hacac at the first stage. Then, on one hand, the Zn(acac)(OH) species can further decompose in the second stage by the rearrangement of an intramolecular proton to form $Zn(OH)_2$. On the other hand, the molecules can react with an extramolecular proton originating from H_2O, EtOH, H_2S and acid, to produce the second Hacac and the Zn-containing intermediate products that can further decompose to ZnO or Zn(O,S), respectively. The proton-promoted thermolysis mechanism explains well the observed acceleration of the decomposition process in the presence of H_2O, EtOH, H_2S as well as acid.

Real time tracking of the intensities of relevant masses by mass spectrometry demonstrates that in the AACVD process H_2S promotes the chemical decomposition and sulfurization of $Zn(acac)_2$ in the gas phase. However, only an adequate amount of H_2S enlarges the film deposition rate. An excess of H_2S depletes the gaseous $Zn(acac)_2$ concentration because it reacts already partially before reaching the substrate surface with the formation of non-adherent and lost solid ZnS particles, and therefore the film growth rate decreases. By understanding the thermal decomposition mechanism, the synthesis conditions can be optimized. This subsequently allows the film properties to be adjusted to meet the requirement of the application in chalcopyrite or kesterite thin film solar cells.

Declaration of Competing Interest

The authors declare that they have no known competing financial interests or personal relationships that could have appeared to influence the work reported in this paper.

Acknowledgement

This work was financially supported by the National Natural Science Foundation of China (Grant Nos.21905057).

Appendix A. Supplementary data

Supplementary data to this article can be found online at https://doi.org/10.1016/j.ultsonch.2021.105492.

References

[1] M. Nakamura, K. Yamaguchi, Y. Kimoto, Y. Yasaki, T. Kato, H. Sugimoto, Cd-Free Cu(In, Ga)(Se, S)(2) thin-film solar cell with record efficiency of 23.35%, IEEE J. Photovolt. 9 (2019) 1863–1867.
[2] R. Klenk, A. Steigert, T. Rissom, D. Greiner, C.A. Kaufmann, T. Unold, M.C. Lux-Steiner, Junction formation by Zn(O, S) sputtering yields CIGSe-based cells with efficiencies exceeding 18%, Prog. Photovoltaics 22 (2014) 161–165.
[3] M. Kriisa, R. Sáez-Araoz, C.-H. Fischer, T. Köhler, E. Kärber, Y. Fu, F. Hergert, M. C. Lux-Steiner, M. Krunks, Study of Zn(O, S) films grown by aerosol assisted chemical vapour deposition and their application as buffer layers in Cu(In, Ga)(S, Se)(2) solar cells, Sol. Energy 115 (2015) 562–568.
[4] L. Huang, J. Li, S. Wang, L. Zhong, X. Xiao, Forming an ultrathin SnS Layer on Cu2ZnSnS4 surface to achieve highly efficient solar cells with Zn(O,S), Buffer. Sol. Rrl. 4 (2020).
[5] Z.-W. Jiang, S.-S. Gao, S.-Y. Wang, D.-X. Wang, P. Gao, Q. Sun, et al., Insight into band alignment of Zn(O, S)/CZTSe solar cell by simulation, Chinese Phys. B 28 (2019).
[6] N. Naghavi, S. Temgoua, T. Hildebrandt, J.F. Guillemoles, D. Lincot, Impact of oxygen concentration during the deposition of window layers on lowering the metastability effects in Cu(In, Ga)Se-2/CBD Zn(S, O) based solar cell, Prog. Photovoltaics 23 (2015) 1820–1827.
[7] T. Ericson, J.J. Scragg, A. Hultqvist, J.T. Watjen, P. Szaniawski, T. Torndahl, et al., Zn(O, S) buffer layers and thickness variations of CdS buffer for Cu2ZnSnS4 solar cells, IEEE J. Photovolt. 4 (2014) 465–469.
[8] Q. Cheng, D. Wang, H. Zhou, Electrodeposition of Zn(O, S) (zinc oxysulfide) thin films: exploiting its thermodynamic and kinetic processes with incorporation of tartaric acid, J. Energy Chem. 27 (2018) 913–922.
[9] C. Platzer-Björkman, T. Törndahl, D. Abou-Ras, J. Malmström, J. Kessler, L. Stolt, Zn(O, S) buffer layers by atomic layer deposition in Cu(In, Ga)Se-2 based thin film solar cells: band alignment and sulfur gradient, J. Appl. Phys. 100 (2006).
[10] S. Merdes, F. Ziem, T. Lavrenko, T. Walter, I. Lauermann, M. Klingsporn, et al., Above 16% efficient sequentially grown Cu(In, Ga)(Se, S)(2)-based solar cells with atomic layer deposited Zn(O, S) buffers, Prog. Photovoltaics 23 (2015) 1493–1500.
[11] C.J. Porter, J.H. Beynon, T. Ast, The modern mass spectrometer—a complete chemical laboratory, Org. Mass Spectrometry 16 (1981) 101–114.
[12] V.V. Krisyuk, A.E. Turgambaeva, I.K. Igumenov, Volatile lead beta-diketonates as CVD precursors, Chem. Vapor. Depos. 4 (1998) 43.
[13] A.F. Bykov, A.E. Turgambaeva, I.K. Igumenov, P.P. Semyannikov, Mass spectrometric study of thermolysis mechanism of metal acetylacetonates vapour, Le Journal De Physique IV 05 (1995). C5-191-C5-7.
[14] H.M. Ismail. A thermoanalytic study of metal acetylacetonates. 1991;21:315-26.
[15] T. Arii, A. Kishi, Humidity controlled thermal analysis - the effect of humidity on thermal decomposition of zinc acetylacetonate monohydrate, J. Therm. Anal. Calorim. 83 (2006) 253–260.
[16] C.G. Macdonald, J.S. Shannon, Mass spectrometry and structures of metal acetylacetonate vapours, Aust. J. Chem. 19 (1966) 1545.
[17] Entry No. 12767, NIST 107 (zinc acetylacetonate, C10H14O4Zn).
[18] Entry No. 19843, NIST 107 (acetylacetone, C5H8O2).
[19] S.E. Gledhill, T.P. Niesen, N.A. Allsop, G. Gimpl, M. Kruger, T. Kohler, et al., Improvement in spray deposition of the intrinsic Zno window layer for chalcopyrite solar cells, in: 2009 34th IEEE Photovoltaic Specialists Conference, 2009, pp. 65–69.
[20] A.J.C. Fiddes, K. Durose, A.W. Brinkman, J. Woods, P.D. Coates, A.J. Banister, Preparation of ZnO films by spray pyrolysis, J. Cryst. Growth 159 (1996) 210–213.
[21] K. Kamata, H. Hosono, Y. Maeda, K. Miyokawa, Synthesis of zinc-oxide powder by hydrolysis of Bis(Acetylacetonato)Zinc(Ii) in aqueous-solution, Chem. Lett. (1984) 2021–2022.
[22] S. Gledhill, R. Allison, N. Allsop, Y. Fu, E. Kanaki, R. Sáez-Araoz, et al., The reaction mechanism of the spray Ion Layer Gas Reaction process to deposit In2S3 thin films, Thin Solid Films. 519 (2011) 6413–6419.
[23] G.L. Marshall, Electron-impact mass-spectrometry of the acetates of zinc, magnesium cobalt and manganese, Org. Mass Spectrom. 18 (1983) 168–172.
[24] R. Vacassy, S.M. Scholz, J. Dutta, C.J.G. Plummer, R. Houriet, H. Hofmann, Synthesis of controlled spherical zinc sulfide particles by precipitation from homogeneous solutions, J. Am. Ceram. Soc. 81 (1998) 2699–2705.
[25] B. Alcaide, N.R. Salgado, M.A. Sierra, New fragmentation and rearrangement reactions of the azetidine ring promoted by AlEt2Cl, Tetrahedron Lett. 39 (1998) 467–470.
[26] E.M. Carreira, T.C. Fessard, Four-membered ring-containing spirocycles: synthetic strategies and opportunities, Chem. Rev. 114 (2014) 8257–8322.